ISBN: 978-3-95450-236-3 ISSN: 2673-7027 doi:10.18429/JACoW-eeFACT2022-MOXAT0103

SuperKEKB LUMINOSITY QUEST*

Y. Ohnishi†, KEK, Tsukuba, Japan
on behalf of the SuperKEKB and Belle II commissioning groups

Abstract

SuperKEKB is a positron-electron collider with a nano-beam scheme and continues to achieve the world's highest luminosity for the production of B meson pairs. The luminosity performance has been improved by the full-scale adoption of the crab-waist scheme. The nano-beam scheme allows the vertical beta function at the interaction point (IP) to be much smaller than the bunch length. The vertical beta function and the beam size at the collision point are the smallest in the world among colliders. As the result, the peak luminosity of $4.65{\times}10^{34}\,\mathrm{cm^{-2}s^{-1}}$ has been achieved with the Belle II detector in 2022. Recent progress will be presented, and then the problems and issues to be overcome from the beam physics point of view will be discussed for further improvement of luminosity performance in the future.

INTRODUCTION

The SuperKEKB accelerator [1, 2] is a positron-electron collider whose main purpose is B meson pair production. The target integrated luminosity is $50\,\mathrm{ab^{-1}}$. The accelerator will be stopped for the first long-term shutdown (LS1) after about 3 years and half of the operation from March 2019, when Phase 3 began, to June 2022. The LS1 will cover upgrades to the Belle II detector [3] and minor modifications to the accelerator. This paper reports on the accelerator performance achieved until 2022. The run from February to the end of March is denoted as *a*, the run from April to July as *b*, and the run from October to December as *c*, with each denoted at the end of the calendar year. The run preceding LS1, the most recent operating period, is represented as 2022b.

The SuperKEKB accelerator consists of an electron ring (HER) with the beam energy of 7 GeV and a positron ring (LER) with the beam energy of 4 GeV, an electron-positron injector [4] with a positron damping ring [5], and beam transport lines connecting them. In the main ring, which has a circumference of about 3 km, the Belle II detector is placed at a collision point.

In order to achieve collisions with asymmetric energies, a double ring is required. It makes to accumulate many bunches while maintaining a single collision point. In addition, a large horizontal crossing angle at the collision point realizes a nano-beam scheme [6, 7]. A final focusing system (QCS) [8] consists of superconducting magnets is placed in the interaction region (IR) to strongly squeeze the beam.

In the LER, ARES RF accelerating cavities [9], which are normal-conducting cavities, are installed, and ARES cavities and superconducting RF accelerating cavities (SCC) [10, 11] are installed in the HER. The linac injector provides beams of the same energy as the main ring with a top-up injection. The energy lost by emitting synchrotron radiation is compensated by the RF cavities. The arc section employs non-interleaved chromaticity correction similar to that of the KEKB accelerator [12], and the emittance can be adjusted in combination with wiggler magnets in the straight sections (OHO and NIKKO). This enables the low emittance required by the nano-beam scheme.

Local chromaticity correction is placed in the straight section (TSUKUBA) where the IR is located, and the chromatic aberration generated in the drift space from the final focus quadrupole magnets to the collision point is efficiently corrected. The sextupole magnets for the local chromaticity correction are also used to perform the crab-waist scheme [13, 14].

The optical functions are calculated by using *SAD* [15] for the model lattice to compare with the measured optical functions and correct them [16]. Typical residual errors after optics corrections are 5 % for the beta functions (rms of $\Delta\beta_{x,y}/\beta_{x,y}$), 5 mm for dispersions (rms of $\Delta\eta_y$). The X-Y couplings as the leakage orbit in the vertical direction from the horizontal single-kick orbit (ratio of rms of Δy to rms of Δx) are obtained to be 0.012–0.016.

LUMINOSITY PERFORMANCE

The highest luminosity achieved through June 2022 is $4.65{\times}10^{34}\,\mathrm{cm^{-2}s^{-1}}$. The unofficial record without data acquisition by the Belle II detector is $4.71{\times}10^{34}\,\mathrm{cm^{-2}s^{-1}}$. These records are more than twice the highest luminosity achieved with the KEKB accelerator. The integrated luminosity provided by the accelerator is $491\,\mathrm{fb^{-1}}$, of which $428\,\mathrm{fb^{-1}}$ ($4\,\mathrm{fb^{-1}}$ is data not used in the analysis) was recorded at the Belle II detector. Table 1 shows the best integrated luminosity records per 8 hours(per shift), per day, and per 7 days.

Table 1: Integrated Luminosity Records

	Recorded	Delivered	Unit
Shift (8 hours)	958	1036	$\mathrm{pb^{-1}}$
1 day	2.5	2.9	$\mathrm{fb^{-1}}$
7 days	15.0	16.6	$\mathrm{fb^{-1}}$

The maximum beam current is 1.46 A for the LER and 1.14 A for the HER. The maximum number of bunches achieved is 2346 which corresponds to about 4 nsec for a 2-bucket spacing. The vertical beta function at the IP is

* WORK SUPPORTED BY KEK, MINISTRY OF EDUCATION, CULTURE, SPORTS, SCIENCE AND TECHNOLOGY (MEXT), AND JSPS KAKENHI GRANT NUMBER 17K05475, JAPAN.
† yukiyoshi.onishi@kek.jp

ISBN: 978-3-95450-236-3   ISSN: 2673-7027   doi:10.18429/JACoW-eeFACT2022-MOXAT0103

mainly 1 mm for the operation, with a minimum value of 0.8 mm. When the vertical beta function at the IP is 0.8 mm, there are issues of beam lifetime and injection efficiency that depend on the optimization of the dynamic aperture with sextupole settings and physical aperture limited by movable collimators [17]. Both rings use the crab-waist scheme, which applies the crab-waist ratio of 80 % for the LER and 40 % for the HER. It is found that the crab-waist scheme reduces the effect of resonance lines that deteriorate luminosity, while significantly reducing the dynamic aperture. The machine parameters that achieved the highest luminosity are shown in Table 2. The σ_y^* shown in Table 2 is estimated by

Table 2: Machine Parameters

	LER	HER	Unit
Emittance, ε_x	4.0	4.6	nm
Beam current, $I_\pm$	1321	1099	mA
Number of bunches, n_b	2249		
Bunch current, $I_{b\pm}$	0.587	0.489	mA
Hor. size at IP, σ_x^*	17.9	16.6	μm
Ver. size at IP, σ_y^*	0.215		μm
Hor. betatron tune, ν_x	44.525	45.532	
Ver. betatron tune, ν_y	46.589	43.573	
Hor. beta at IP, β_x^*	80	60	mm
Ver. beta at IP, β_y^*	1.0	1.0	mm
Piwinski angle, Φ	10.7	12.7	
Crab-waist ratio	80	40	%
Beam-Beam, ξ_y	0.041	0.028	
Luminosity, L	4.65×10^{34}		1/cm^2/s

the Σ_y^* calculated from the luminosity divided by $\sqrt{2}$ with assuming $\sigma_{y+}^* = \sigma_{y-}^*$. The bunch length, σ_z used in the calculation is a nominal value. Luminosity is

$$L = \frac{N_+ N_- n_b f_0}{2\pi\phi_x \Sigma_z \Sigma_y^*}, \tag{1}$$

where $N_\pm$ is a number of particles, f_0 is a revolution frequency,

$$\Sigma_z = \sqrt{\sigma_{z+}^2 + \sigma_{z-}^2} \quad \text{and} \quad \Sigma_y^* = \sqrt{\sigma_{y+}^{*2} + \sigma_{y-}^{*2}}. \tag{2}$$

Piwinski angle is defined by

$$\Phi = \frac{\sigma_z}{\sigma_x^*} \tan\phi_x, \tag{3}$$

where ϕ_x is a half crossing-angle of 41.5 mrad. A feature of the nano-beam scheme is that the Piwinski angle is 10 or more, which is about 10 times larger than that of conventional colliders. This allows the vertical beta function at the IP to be squeezed to the bunch length divided by the Piwinski angle. However, the effect of bunch length on luminosity is introduced, so the vertical beam size needs to be reduced to compensate for the reduction of geometrical luminosity. The nominal bunch length is 4.6 mm for the LER and 5.1 mm for the HER. Practically, the bunch length is measured to be about 6 mm at the bunch current of 0.4 mA in the LER.

Crab-Waist Scheme

The advantage of the crab-waist scheme is not only to compensate for geometric luminosity loss but also to reduce betatron or synchro-betatron resonances caused by beam-beam interactions [18, 19]. For a crab-waist ratio of 100 %, the required K value (1/m^2) of a sextupole magnet is

$$K_2 = \frac{1}{\cos\Delta\psi_x \sin^2\Delta\psi_y} \frac{1}{\tan 2\phi_x} \frac{1}{\beta_y^s \beta_y^*} \sqrt{\frac{\beta_x^*}{\beta_x^s}}, \tag{4}$$

where β_x^s and β_y^s are the beta functions at the crab-waist sextupole magnet, and $\Delta\psi_{x,y}$ is the phase advance to the IP. The phase advances are designed and adjusted to have $|\cos\Delta\psi_x| = 1$ and $\sin^2\Delta\psi_y = 1$. The crab-waist scheme enables collision experiments with high bunch currents and improves specific luminosity [20, 21].

Specific Luminosity

Figure 1 shows the relationship between the specific luminosity and the bunch current product. The cases where $\beta_y^* = 1$ mm and 0.8 mm are shown. The specific luminosity is expressed by

$$L_{sp} = \frac{L}{n_b I_{b+} I_{b-}} \propto \frac{1}{\Sigma_z \Sigma_y^*}. \tag{5}$$

The beam size is constant with respect to the bunch current product unless a blowup occurs. It has been found that even with the setting of 1 mm, the deviation of the horizontal beam orbit in the local chromaticity correction causes a beta-beat and a deviation of the vertical beta function at the IP. In this case, the estimated beta function at the IP is also shown in the figure. This is more significant for the HER than for the LER.

In the case of $\beta_y^* = 0.8$ mm, higher specific luminosity was obtained with the bunch current product of 0.05 mA^2, but it decreases sharply around 0.1 mA^2. This may suggest that the correction of chromatic X-Y couplings is not optimized enough.

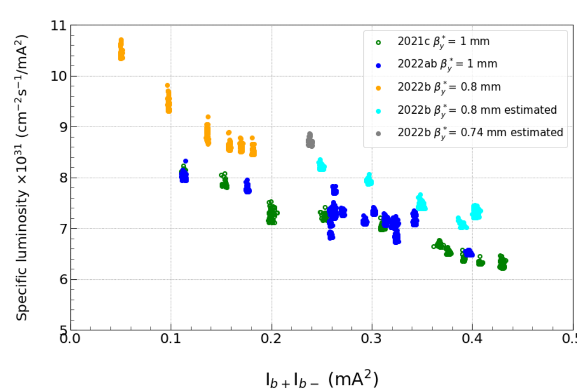

Figure 1: Specific luminosity.

ISBN: 978-3-95450-236-3 ISSN: 2673-7027 doi:10.18429/JACoW-eeFACT2022-MOXAT0103

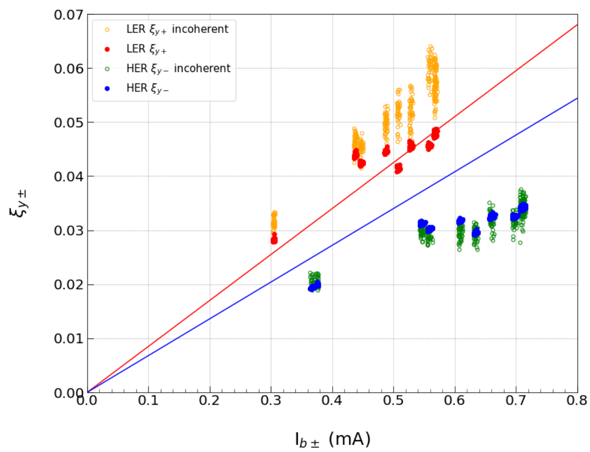

Figure 2: Beam-Beam parameter for the LER and HER, respectively. The red line shows calculated beam-beam parameter in the LER and blue line for the HER without a beam-beam blowup where the vertical emittance is 25 pm in the LER and 40 pm in the HER.

Beam-Beam Interaction

As squeezing the vertical beta function at the IP, the vertical beam-beam parameter decreases, usually according to $\sqrt{\beta_y^*}$. However, if the vertical emittance can also be reduced in proportion to β_y^*, the beam-beam parameter remains constant for the same bunch current. In other words, the luminosity increases only by $1/\sqrt{\beta_y^*}$ when β_y^* is squeezed, but if the vertical emittance can be decreased at the same time, the luminosity improves proportional to $1/\beta_y^*$. Figure 2 shows the beam-beam parameters for the bunch current of the opposite beam. The figure shows two types of beam-beam parameters in the physics run. The beam-beam parameters calculated from the luminosity is

$$\xi_{y\pm} = 2er_e \frac{\beta_{y\pm}^* L}{\gamma_\pm I_\pm}. \tag{6}$$

On the other hand, the incoherent beam-beam parameter is written by

$$\xi_{y\pm} = \frac{r_e}{2\pi\gamma_\pm}\left(\frac{I_{b\mp}}{ef_0}\right)\frac{\beta_{y\pm}^*}{\phi_x\sigma_{z\mp}\sigma_{y\mp}^*} \propto I_{b\mp}\sqrt{\frac{\beta_{y\pm}^*}{\varepsilon_{y\mp}}}, \tag{7}$$

where $\beta_{y+}^* = \beta_{y-}^*$. The reason why the beam-beam parameters of the HER are smaller than those of the LER is mainly because the beam current of the HER is increased compared to the energy ratio in the process of optimizing luminosity. When the HER beam current becomes smaller, the HER beam size tends to a blowup. In the bunch current region (0.8 mA or less) used in the physical run, the optimum ratio of the LER to the HER is 5 : 4. When the beam current is increased while maintaining this current ratio, the increase of beam-beam parameter in the electron beam slows down when the LER bunch current exceeds 0.6 mA. The highest beam-beam parameter seems to be 0.03 to 0.035 for the physics run. However, in the high-bunch current collision study with a small number of bunches, an optimization was performed specifically for the luminosity performance, the beam-beam parameter of 0.045 was achieved.

Correction of Chromatic X-Y Couplings in the LER

The LER is equipped with sextupole magnets rotating around the beam axis of 6 families on each side across the IP [22]. Both of chromatic X-Y couplings at the IP and chromaticity can be corrected by the rotatable sextupole magnets. There are four parameters for the X-Y couplings: r_1, r_2, r_3, and r_4. The chromatic X-Y couplings of r_1' and r_2', which have a direct effect on the luminosity, were corrected. To estimate the magnitude of the chromatic X-Y couplings, we focus on the resonance-line strengths $\nu_x - \nu_y - \nu_s$ =integers and $\nu_x - \nu_y - 2\nu_s$ =integers. Fix the horizontal tune, the vertical tune was scanned with measuring the vertical beam size by using the X-ray beam size monitor (XRM) [23]. Figures 3 and 4 show the relationship between the measured vertical emittance and the vertical tune (in the model) when r_1' and r_2' at the IP are changed. Based on these measurements, we decided to adopt $r_1' = -1$ and $r_2' = 0$ m as the combination with the weakest resonance-line strength.

OBSTACLES TO LUMINOSITY IMPROVEMENT

Beam Blowup in the LER

No beam blowup due to electron cloud effect in the LER was observed up to 0.35 mA/bunch/bucket spacing which corresponds to the maximum beam current of 1.64 A. However, the blowup for single-beam and single-bunch have been observed [24]. When observing the tune spectrum, the -1 mode side band ($\nu_y - \nu_s$) appears with a high bunch current. This -1 mode instability is thought to be related to the beam blowup, but the whole picture has not been fully understood. There are three sources of -1 mode instability; the impedance due to the movable collimators, the tuning of the bunch-by-bunch feedback system, and the vertical

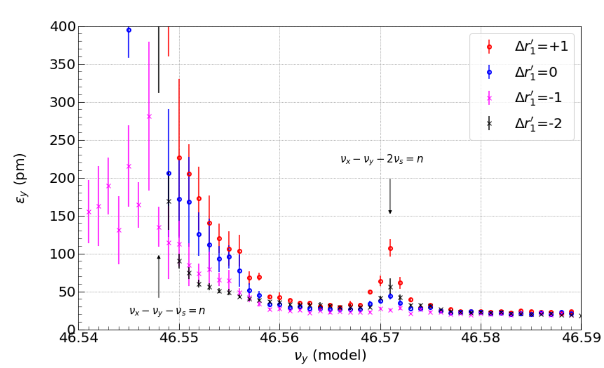

Figure 3: Vertical emittance as a function of vertical tune with different r_1'.

ISBN: 978-3-95450-236-3 ISSN: 2673-7027 doi:10.18429/JACoW-eeFACT2022-MOXAT0103

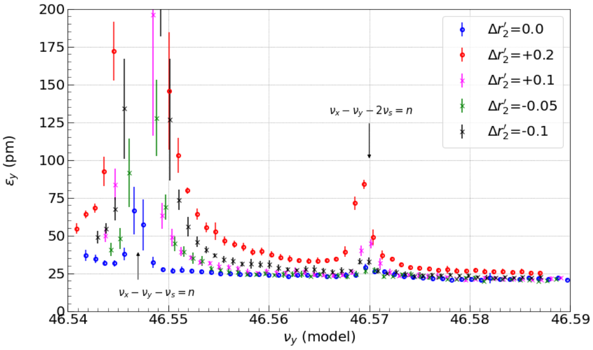

Figure 4: Vertical emittance as a function of vertical tune with different r_2'. The unit of $\Delta r_2'$ is m.

tune. After minimizing the impedance of the collimators and adjusting the bunch-by-bunch feedback system, it has been demonstrated that the beam blowup can be suppressed. In particular, simulation results show that reducing the number of taps in the bunch-by-bunch feedback system does not induce the blowup due to -1 mode instability. Selecting a higher vertical tune also helps to suppress the beam blowup.

It has been observed that when the collimator head is damaged by large beam loss, the bunch current dependence of the vertical tune shift increases. A damaged collimator is assumed to have an increased impedance. Collimator damage causes the beam blowup and increases beam backgrounds, which is a serious problem in the accelerator operation.

Sudden Beam Loss

There are events that cause beam loss in a few turns and lead to beam abort. In most cases, the beam loss is detected and the beam is aborted by the loss monitor, but if the amount of beam loss is too large, it causes damage to the collimator head and QCS quench. It is observed that the fast beam loss occurs near these collimators. We call the fast beam loss "sudden beam loss".

For the LER, we mainly use three movable collimators in the vertical direction, D06V1, D06V2, and D02V1, from the upstream of the IP. A large beam loss near D02V1 often quenches the QCS and increases the dose in the Belle II detector. Among the QCS, the superconducting coil for the LER called QC1LP, which is the closest to the downstream of the IP, is quenched, and in the case of a larger beam loss, the superconducting coil called QC1RP on the upstream side is also quenched. It can also damage the D06V1 and D02V1 collimator heads. Simultaneously, a vacuum pressure rise near the collimator is observed. The superconducting coil for the HER has never been quenched during the normal accelerator operation. Large sudden beam losses tend to become noticeable when the LER bunch current exceeds 0.7 mA. Also, if the collimator head is damaged and the impedance increases, the bunch current threshold that causes such sudden and large beam loss tends to be low.

Collimator Impedance

A movable collimator plays a major role in reducing the beam background for the Belle II detector. The beam background is caused by injected beams and stored beams [25]. For the stored beam, the beam background is caused by a scattering due to residual gas in the vacuum pipes, a particle scattering in a bunch, and a scattering due to collisions with opposite beams which becomes more pronounced as the luminosity increases. Residual gas decreases as the vacuum baking progresses. For the low emittance, a probability of intra-beam scattering increases and the dynamic aperture of the optics containing the IP decreases, so that the scattered particles move out of the stable region and become the background. If the emittance or energy spread of the injected beam is larger than required, or if the coherent oscillation due to the top-up injection is large, the injected beam causes the background. The physical aperture of the movable collimator is adjusted to reduce these beam backgrounds. In that case, an optimization is performed while balancing injection efficiency and beam lifetime. Compared to the horizontal collimator, the physical aperture of the vertical collimator is considered to be very small and the impedance is large since the vertical aperture of QC1s determines the physical aperture.

The short-range wake field due to the movable collimators makes single-bunch tune shift. The vertical tune shift is expressed by

$$\frac{\Delta \nu_y}{I_b} = -\frac{T_0}{4\pi(E/e)} \sum_i \beta_{yi} \kappa_i(d), \tag{8}$$

where T_0 is the revolution frequency (about 10 μsec), $\kappa_i(d)$ is the loss factor of each movable collimator which is a function of physical aperture of d. Figure 5 shows the relationship between the measured bunch current dependence of the vertical tune-shift in the LER and the estimated product of the loss factor and β_y at the vertical collimator for each β_y^*. If the impedance near QCS is dominant, there should be a difference in the tune shift due to the beta function at the IP, but this is not observed. On the other hand, it can be seen that the change in impedance due to the physical aperture of the collimator has a significant effect on the tune shift. In the physics run, the sum of $\beta_y \kappa(d)$ of the LER is about 33 kV/pC and the tune shift is about -0.011 mA^{-1} which corresponds to about half of the synchrotron tune in the LER. However, as described in the previous section, if a large beam loss occurs and the collimator head is damaged, the tune shift becomes further larger.

Optics Changes due to Beam-Line Deformation

In the HER, a significant vertical tune shift was observed with increasing beam current. Recently, it has been found that the horizontal orbit at strong sextupole magnets deviates from the reference orbit with the beam current, even with performing the continuous closed orbit correction (CCC) every 15 seconds. The deviation of the horizontal orbit in the sextupole magnet causes a tune shift due to create a quadrupole

ISBN: 978-3-95450-236-3 ISSN: 2673-7027 doi:10.18429/JACoW-eeFACT2022-MOXAT0103

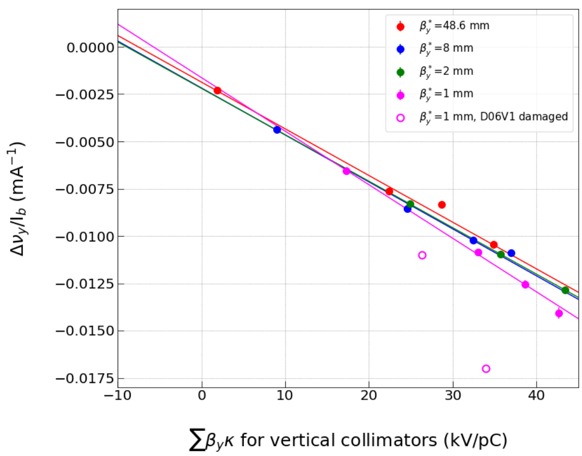

Figure 5: Slope of vertical tune as a function of $\sum \beta_y \kappa$.

magnetic field component. In particular, in the case of sextupole magnets for the local chromaticity correction, the horizontal beta function is small and the vertical beta function is large. Therefore, mainly the vertical tune shift occurs. Assuming that as the beam current increases, the beam line is deformed by the synchrotron radiation heating and the deviation of the orbit in the horizontal direction increases, the resulting vertical tune shift is consistent with the measured value. We observed the horizontal tune shift which can be explained by resistive wall impedance. Tune shift due to the resistive wall impedance should also contribute in the vertical direction. Regarding the vertical tune shift, amount of the tune shift due to the horizontal orbit deviation at the sextupole magnet and the resistive wall impedance is not clear, so further detailed investigation is required.

The quadrupole magnetic field components produced by horizontal orbital deviations at strong sextupole magnets cause beta-beats as well as tune shifts. As a result of beta-beat, the vertical beta function at the IP also changes. In the case of the HER, as the beam current increases, the horizontal beam orbit at the pair of sextupole magnets in the local chromaticity correction tends to shift toward the outside of the ring. The orbit deviation is in the direction that the vertical beta function at the IP becomes smaller, and with a shift of 20 μm, β_y^*=1 mm is reduced to be about 0.8 mm. A local bump orbit placed at the sextupole magnet is used to correct horizontal beam orbit deviations. As a result, the reproducibility of optics corrections at low current (50 mA) was improved. In addition, the injection efficiency in the high current region recovered to the same level as that in the low current region, and the beam background was reduced. The vertical beta function in the arc section is smaller compared to the local chromatic aberration correction, but there are strong sextupole magnets in the arc. Further more, the vertical orbit deviation at the sextupole magnet produces X-Y couplings. Since there is a similar problem in the LER, we should understand the deformation of the beam line as a whole ring, and consider the system that keeps the beam orbit constant in the entire beam current at the level of 10 μm order.

Lifetime and Beam Injection

The characteristics of the nano-beam scheme are low emittance and small beta function at the IP. These make it difficult to ensure sufficient dynamic aperture. Simulations show that the crab-waist scheme reduces the dynamic aperture for particles with momentum deviations. The physical aperture of the movable collimator for beam background reduction also affects the beam lifetime. If the vertical beta function at the IP is squeezed, the injection efficiency decreases. Moreover, since the injection efficiency depends on the bunch current, the beam-beam effect can not be ignored for the injection. In the future, it will be a big challenge to squeeze the beta functions at the IP and increase the beam current to achieve a luminosity exceeding 10^{35} cm^{-2}s^{-1}.

SUMMARY

The recent operation status of the SuperKEKB accelerator was reported in this article. In the operation of 2022*b*, the LER beam current exceeded 1 A and became stable, then the maximum beam current reached 1.4 A. The number of bunches could be increased to 2346 bunches (2-bucket spacing). As a result, the maximum luminosity of $4.65{\times}10^{34}$ cm^{-2}s^{-1} was achieved. Figure 6 shows the history of the beam current, luminosity and integrated luminosity. The accelerator was operated as Phase 3 from spring in 2019 to summer in 2022, but it entered a long-term shutdown (LS1) after that. The accelerator will be upgraded, including the adoption of a nonlinear collimator and the modification of vacuum pipe at injection region in the HER in LS1. We plan to achieve 10^{35} cm^{-2}s^{-1} within 2 years after LS1 and an integrated luminosity of 15 ab^{-1} in 10 years.

ACKNOWLEDGMENTS

We would like to thank all those involved in the operation of the SuperKEKB accelerator. The research results were widely supported by the INFN(LNF), CERN, and KEK collaborations, for which we would like to thank them here.

REFERENCES

[1] Y. Ohnishi *et al.*, *Prog. Theor. Exp. Phys.*, vol. 2013, p. 03A011, 2013. doi:10.1093/ptep/pts083

[2] K. Akai *et al.*, *Nucl. Instrum. Methods*, vol. A907, p. 188, 2018. doi:10.1016/j.nima.2018.08.017

[3] Belle II, *Technical Design Report*, 2010. arXiv:1011.0352.

[4] K. Furukawa *et al.*, in *Proc. IPAC'18*, Vancouver, Canada, Apr.-May 2018, pp. 300–303. doi:10.18429/JACoW-IPAC2018-MOPMF073

[5] M. Kikuchi *et al.*, in *Proc. IPAC'10*, Kyoto, Japan, May 2010, paper TUPEB054, pp. 1641–1643.

[6] P. Raimondi, Presented at the 2nd Workshop on Super B-Factory, Frascati, 2006.

[7] *SuperB Conceptual Design Report*, INFN/AE-07/2, SLAC-R-856, LAL 07-15 March, 2007.

ISBN: 978-3-95450-236-3 ISSN: 2673-7027 doi:10.18429/JACoW-eeFACT2022-MOXAT0103

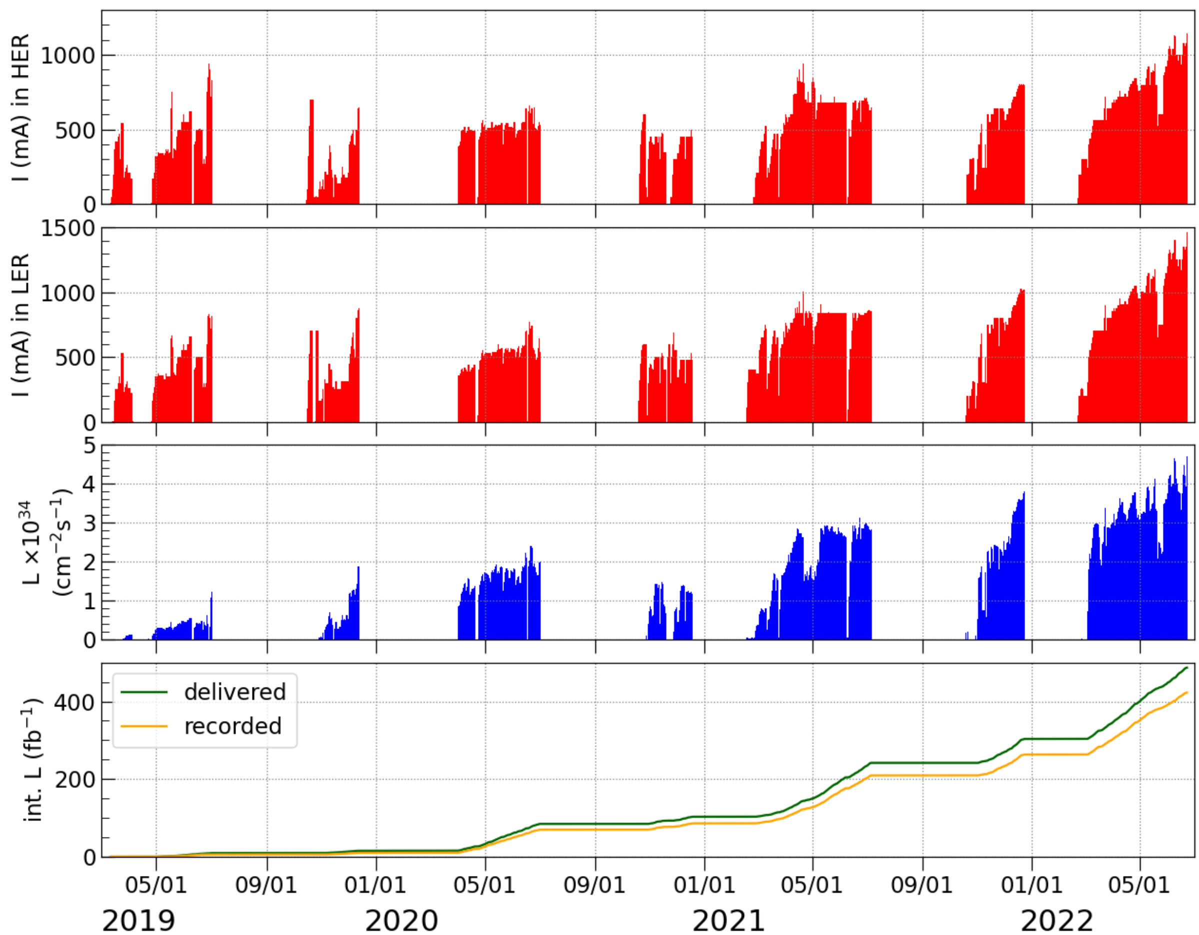

Figure 6: History of SuperKEKB since 2019.

[8] N. Ohuchi *et al.*, in *Proc. IPAC'18*, Vancouver, Canada, Apr.-May 2018, pp. 1215–1219. doi:10.18429/JACoW-IPAC2018-TUZGBE2

[9] K. Watanabe *et al.*, in *Proc. IPAC'19*, Melbourne, Australia, May 2019, pp. 619–621. doi:10.18429/JACoW-IPAC2019-MOPRB022

[10] T. Furuya *et al.*, in *Proc. SRF'95*, Gif-sur-Yvette, France, Oct.1995, paper SRF95F35, pp. 729–733.

[11] T. Tajima *et al.*, in *Proc. 2nd Superconducting Linear Accelerator Meeting in Japan*, KEK-PROC–99-25.

[12] T. Abe *et al.*, *Prog. Theor. Exp. Phys.*, vol. 2013, p. 03A001, 2013. doi:10.1093/ptep/pts102

[13] *SuperB Conceptual Design Report*, INFN/AE-07/2, SLAC-R-856,LAL 07-15 March, 2007.

[14] K. Oide *et al.*, *Phys. Rev. Accel. Beams*, vol. 19, p. 111005, 2016. doi:10.1103/PhysRevAccelBeams.19.111005

[15] *Strategic Accelerator Design*, http://acc-physics.kek.jp/SAD.

[16] H. Sugimoto *et al.*, in *Proc. eeFACT2022*, Frascati, Italy, Sep. 2022. Paper TUXAT0103, this conference

[17] T. Ishibashi *et al.*, *Phys. Rev. Accel. Beams*, vol. 23, p. 053501, 2020. doi:10.1103/PhysRevAccelBeams.23.053501

[18] M. Zobov *et al.*, *Phys. Rev. Lett.*, vol. 104, p. 174801, 2010. doi:10.1103/PhysRevLett.104.174801

[19] D. Shatilov *et al.*, *Phys. Rev. ST Accel. Beams*, vol. 14, p. 014001, 2011. doi:10.1103/PhysRevSTAB.14.014001

[20] Y. Ohnishi *et al.*, *Eur. Phys. J. Plus*, vol. 136, p. 1023, 2021. doi.org/10.1140/epjp/s13360-021-01979-8

[21] D. Zhou *et al.*, in *Proc. IPAC'22*, Bangkok, Thailand, Jun. 2022, pp. 2011–2014. doi:10.18429/JACoW-IPAC2022-WEPOPT064

[22] R. Sugahara *et al.*, *IEEE Trans. Appl. Supercond.*, vol. 26, 2016. doi:10.1109/TASC.2016.2534760

[23] J. W. Flanagan, in *Proc. IBIC'18*, Shanghai, China, Sep. 2018, pp. 361–365. doi:10.18429/JACoW-IBIC2018-WEOC02

[24] S. Terui *et al.*, in *Proc. IPAC'22*, Bangkok, Thailand, Jun. 2022, pp. 2169–2172. doi:10.18429/JACoW-IPAC2022-WEPOTK050

[25] H. Nakayama *et al.*, in *Proc. IPAC'21*, Campinas, Brazil, May 2021, pp. 2532–2535. doi:10.18429/JACoW-IPAC2021-WEXA07